

## Supporting Information

### A New Fully Bridged Spirophenylacridine Derivative: Synthesis and Characterization

*Shi-Jie Ge<sup>a‡</sup>, Yue-Jian Yang<sup>a‡</sup>, Rui-Hong Liu<sup>a</sup>, You-Jun Yu<sup>a</sup>, Rehman-Mehvish Abdul<sup>a</sup>, Hai-Xiao Jiang<sup>b</sup>, Wei Gao<sup>a</sup>, Dong-Ying Zhou<sup>a</sup>, and Zuo-Quan Jiang<sup>a\*</sup>*

<sup>a</sup> State Key Laboratory of Bioinspired Interfacial Materials Science, Institute of Functional Nano & Soft Materials (FUNSOM), Soochow University, Suzhou, 215123, Jiangsu, PR China. E-mail: zqjiang@suda.edu.cn

<sup>b</sup> School of Chemistry and Life Sciences, Suzhou University of Science and Technology, Suzhou, 215009, Jiangsu, China.

### Table of Contents

1. General information .....	S2
2. Experimental section .....	S4
3. NMR spectra .....	S7
4. Crystal .....	S13
5. Thermal and electrochemical properties .....	S15
6. Photophysical properties .....	S17
7. Theoretical calculations .....	S18
8. Electroluminescence properties .....	S26
9. Reference .....	S29

## 1. General information

All chemicals and reagents were used as supplied by commercial sources without further purification.  $^1\text{H}$  NMR and  $^{13}\text{C}$  NMR spectra were recorded on a Bruker 400 at room temperature. Mass spectra were obtained using a Thermo ISQ mass spectrometer with a direct exposure probe and a Bruker Autoflex II/Compass 1.0, respectively. Thermogravimetric analysis (TGA) was conducted on a TA SDT 2960 instrument at a heating rate of 10 °C/min under nitrogen, with the decomposition temperature ( $T_d$ ) defined as the temperature at 5% weight loss.

Single crystals were obtained by slow evaporation of  $\text{CH}_2\text{Cl}_2/\text{EtOH}$  solutions. X-ray diffraction data were collected using a Bruker D8-Venture diffractometer with a Turbo X-ray source (Mo-K $\alpha$  radiation,  $\lambda = 0.71073 \text{ \AA}$ ) and a CMOS detector at low temperatures. The structure was solved using the XT<sup>1</sup> program with intrinsic phasing, refined using the ShelXL<sup>1</sup> refinement package, and analyzed with Olex2<sup>2</sup>. CCDC entries (2411674 and 2411672) contain supplementary crystallographic data, available free of charge from the Cambridge Crystallographic Data Centre.

Electrochemical measurements were performed using a CHI760 voltammetric analyzer, employing a conventional three-electrode configuration with a platinum working electrode, a platinum-wire counter electrode, and an Ag/AgCl reference electrode. The solvent used was  $\text{CH}_2\text{Cl}_2$ , with 0.1 M tetrabutylammonium hexafluorophosphate as the supporting electrolyte. Ferrocene was added as an internal standard for each set of measurements, and all reported potentials are referenced to the ferrocene-ferrocenium ( $\text{Fc}/\text{Fc}^+$ ) couple, with a scan rate of 100 mV/s. IP and EA energies were calculated using the formulas  $\text{IP} = -[4.8 + E_{\text{O}} - E(\text{Fc}/\text{Fc}^+)] \text{ eV}$ ,  $\text{EA} = -[4.8 + E_{\text{R}} - E(\text{Fc}/\text{Fc}^+)] \text{ eV}$ , and the energy gap ( $E_g$ ) was obtained as  $E_g = \text{EA} - \text{IP}$ .

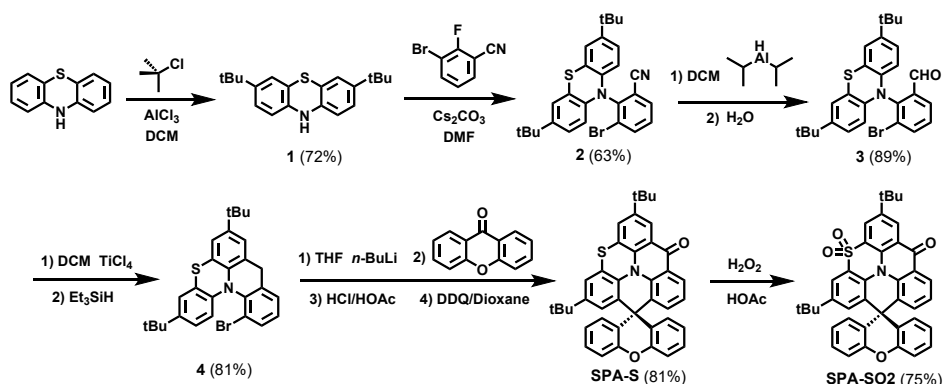
UV-vis absorption spectra were measured on a Shimadzu UV 2600 spectrophotometer. Photoluminescence (PL) and phosphorescence spectra were obtained using a Hitachi F-4600 fluorescence spectrophotometer or a Horiba JY FL-3 spectrophotometer. Absolute PLQY values were measured with a Hamamatsu C9920-02G system in an integrating sphere under a nitrogen atmosphere, with a measurement range of 300–950 nm. Transient spectra were recorded using a Quantaurus-Tau fluorescence lifetime measurement system (C11367-03, Hamamatsu Photonics Co.) in a vacuum.

Ground state, excited states, reorganization energy, hole-electron distributions, electrostatic potential map, and spin-orbit coupling (SOC) matrix elements were calculated at the B3LYP/def2-SVP level using Gaussian 16 program<sup>3</sup>. Molecular orbitals and electron-hole distributions were visualized using the Visual Molecular Dynamics (VMD) software<sup>4</sup>. The molecular orbitals were mapped to represent the spatial distribution of electron densities, while the electron-hole analysis provided

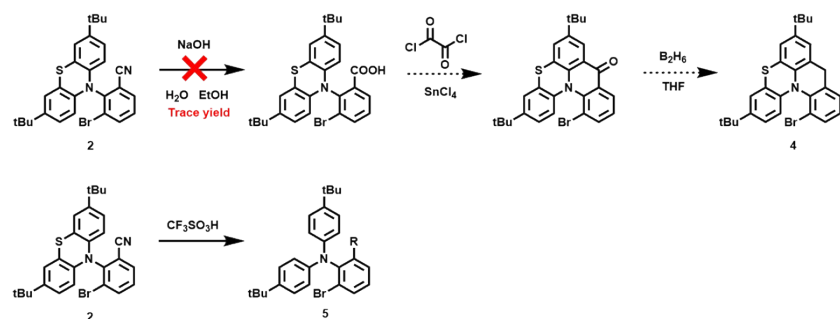
insights into charge separation and recombination processes. Excited state property analysis, two-dimensional iso-chemical shielding surfaces, and calculation of the effective volume and polarizability of atoms were analyzed using the Multiwfn program<sup>5</sup>. At the same time, SOC matrix elements were predicted using the PySOC program<sup>6</sup>.

Electroluminescent devices were fabricated via vacuum deposition technology. All functional layers were deposited on pre-treated ITO substrates. The glass substrates with ITO layers were sequentially cleaned ultrasonically with acetone and ethanol, followed by drying at 110 °C for 1 hour. After ultraviolet–ozone plasma treatment, the substrates were transferred into the evaporation chamber. Electroluminescent fabrication was carried out under a vacuum of  $4 \times 10^{-6}$  Torr. After the deposition of functional layers, electroluminescent characterization, including electroluminescence (EL) spectra, luminance, and current density–voltage–luminance measurements, were performed at room temperature using a Keithley 2400 Source Meter and a Photo Research PR 655 spectrophotometer.

## 2. Experimental section



**Scheme S1.** Synthetic routes for SPA-S and SPA-SO<sub>2</sub>.



**Scheme S2.** Previously investigated synthetic routes.

**Synthesis of 3,7-di-tert-butyl-10H-phenothiazine (1)** was synthesized according to the literature<sup>7</sup>.

### Synthesis of 3-bromo-2-(3,7-di-tert-butyl-10H-phenothiazin-10-yl)benzonitrile (2)

A round-bottom flask equipped with a condenser and a magnetic stirrer bar was charged with 3-bromo-2-fluorobenzonitrile (10 g, 50.08 mmol), compound 1 (13 g, 41.47 mmol), cesium carbonate (27.2 g, 83.47 mmol), and *N,N*-dimethylformamide (600 mL). The mixture was refluxed for 12 hours under nitrogen. Monitoring the reaction completion by TLC. After cooling to room temperature, the reaction mixture was filtered and washed with dichloromethane. The solvent was then distilled under reduced pressure. The reaction mixture was recrystallized with ethanol to obtain a yellow product without further purification. The final product was obtained with a yield of 13.0 g (63%).  $^1\text{H}$  NMR (400 MHz, Chloroform-*d*)  $\delta$  8.08 (dd, *J* = 8.2, 1.4 Hz, 1H), 7.88 (dd, *J* = 7.8, 1.5 Hz, 1H), 7.49 (t, *J* = 8.0 Hz, 1H), 7.05 (d, *J* = 2.3 Hz, 2H), 6.87 (dd, *J* = 8.6, 2.3 Hz, 2H), 5.90 (d, *J* = 8.6 Hz, 2H), 1.23 (s, 18H).  $^{13}\text{C}$  HMR (101 MHz, Chloroform-*d*)  $\delta$  146.1, 142.8, 139.2, 138.0, 134.0, 130.1, 128.7, 124.1, 123.8, 119.7, 115.5, 114.4, 34.1, 31.2. MS (EI) m/z: 492.40 [M $^+$ ]. Calcd for C<sub>27</sub>H<sub>27</sub>BrN<sub>2</sub>S: 491.49

### Synthesis of 3-bromo-2-(3,7-di-tert-butyl-10H-phenothiazin-10-yl)benzaldehyde (3)

Under nitrogen atmosphere, a reaction flask equipped with a magnetic stirrer was

charged with compound 2 (8.0 g, 16.28 mmol) and dichloromethane (60 mL). The mixture was cooled to -78 °C, followed by the addition of diisobutylaluminum hydride (2.78 g, 19.53 mmol). The temperature was raised to -40 °C during 1 hour, and water (7.33 g, 406.92 mmol) was added. The reaction was allowed to warm to 0 °C and stirred for an additional hour. Upon completion, magnesium carbonate and potassium carbonate were added, and the reaction mixture was filtered and washed with dichloromethane. The residue was washed with dichloromethane, and the solvent was removed under reduced pressure. The crude product was purified by column chromatography on silica gel using petroleum ether/dichloromethane (3/2, v/v) as the eluent, yielding an orange-red solid. The final product was obtained with a yield of 7.2 g (89%). <sup>1</sup>H NMR (400 MHz, Chloroform-*d*) δ 10.29 (s, 1H), 8.14 (dq, *J* = 7.8, 1.6 Hz, 2H), 7.55 (t, *J* = 7.9 Hz, 1H), 7.05 (d, *J* = 2.3 Hz, 2H), 6.85 (dd, *J* = 8.6, 2.3 Hz, 2H), 5.92 (d, *J* = 8.6 Hz, 2H), 1.25 (s, 18H). <sup>13</sup>C NMR (101 MHz, Chloroform-*d*) δ 190.7, 146.1, 142.6, 140.4, 139.3, 137.8, 130.3, 128.6, 128.0, 124.0, 119.1, 115.0, 34.1, 31.2. MS (EI) m/z: 495.11 [M<sup>+</sup>]. Calcd for C<sub>27</sub>H<sub>28</sub>BrNOS: 494.49

#### **Synthesis of 13-bromo-3,7-di-tert-butyl-9H-quinolino[3,2,1-kl]phenothiazine (4)**

Under nitrogen protection, compound 3 (4.0 g, 8.09 mmol) and dichloromethane (60 mL) were added to a round-bottom flask equipped with a magnetic stirrer. Titanium tetrachloride (6.14 g, 32.36 mmol) was slowly added at 0 °C, and the mixture was stirred at room temperature for 24 hours. Triethyl silane (3.74 g, 32.19 mmol) was then added, and the reaction was continued for an additional 12 hours. The reaction completion was monitored by TLC. After quenching the reaction with methanol, the solvent was removed under reduced pressure. The residue was purified by column chromatography on silica gel using petroleum ether/dichloromethane (2/3, v/v) as the eluent, yielding a white solid. The final product was obtained with a yield of 3.1 g (81%). <sup>1</sup>H NMR (400 MHz, Chloroform-*d*) δ 7.50 (dt, *J* = 8.0, 1.2 Hz, 1H), 7.35 (d, *J* = 2.2 Hz, 1H), 7.26 (dt, *J* = 7.5, 1.3 Hz, 1H), 7.20 (dd, *J* = 2.0, 0.9 Hz, 1H), 7.14 (dd, *J* = 8.5, 2.2 Hz, 1H), 7.08 – 6.97 (m, 2H), 6.75 (d, *J* = 8.4 Hz, 1H), 4.11 (d, *J* = 17.5 Hz, 1H), 3.83 (d, *J* = 17.7 Hz, 1H), 1.31 (d, *J* = 4.4 Hz, 18H). <sup>13</sup>C NMR (101 MHz, Chloroform-*d*) δ 147.6, 146.8, 141.0, 138.0, 133.6, 132.6, 127.6, 126.5, 125.9, 125.1, 123.9, 122.9, 122.2, 118.1, 116.0, 34.4, 34.4, 33.1, 31.4, 31.4, 27.0. MS (EI) m/z: 479.11 [M<sup>+</sup>]. Calcd for C<sub>27</sub>H<sub>28</sub>BrNS: 478.49

#### **Synthesis of 2,6-di-tert-butyl-12H-spiro[benzo[9,1]quinolizino[3,4,5,6,7-klmn]phenothiazine-8,9'-xanthen]-12-one (SPA-S)**

Under nitrogen conditions, compound 4 (2.0 g, 4.18 mmol) was dissolved in dehydrated tetrahydrofuran and the mixture was cooled to -78 °C for 10 minutes. Then 1.6 M n-BuLi (294.5 mg, 4.60 mmol) was slowly added and the mixture was stirred at -78 °C for 1 h. After that, xanthone (0.98 g, 5.02 mmol) was added and the mixture was stirred at room temperature overnight. Then 10 mL of methyl alcohol was added to quench the reaction. The mixture was concentrated under reduced pressure to remove the organic

solvent. The residue was dissolved in 100 mL glacial acetic acid and then 5 mL HCl was added. The mixture was stirred at 110 °C overnight. After cooling to room temperature, the mixture was concentrated under reduced pressure. The solid was dissolved in a solution of 300 mL 1,4-dioxane/dichloromethane/water (8/4/1, v/v/v). After DDQ (2.36 g, 10.38 mmol) was added at 0 °C, the mixture was stirred at room temperature for 8h. The reaction mixture was concentrated under reduced pressure. Then extracted with dichloromethane and the solvent was removed under reduced pressure, and then the residue was purified by column chromatography on silica gel using petroleum ether/dichloromethane (1/4, v/v) as eluent, the orange solid was finally obtained. The final product was obtained with a yield of 2.0 g (81%). <sup>1</sup>H NMR (400 MHz, Chloroform-*d*) δ 8.46 (dd, *J* = 7.8, 1.9 Hz, 1H), 8.28 (d, *J* = 2.6 Hz, 1H), 7.38 (d, *J* = 2.6 Hz, 1H), 7.34 (dd, *J* = 7.5, 1.9 Hz, 1H), 7.24 – 7.13 (m, 5H), 6.92 – 6.83 (m, 4H), 6.82 (d, *J* = 2.4 Hz, 1H), 6.67 (d, *J* = 2.4 Hz, 1H), 1.40 (s, 9H), 1.01 (s, 9H). <sup>13</sup>C NMR (101 MHz, Chloroform-*d*) δ 177.3, 149.2, 148.4, 147.6, 138.5, 135.0, 133.8, 133.1, 132.7, 131.4, 130.8, 129.3, 128.6, 128.2, 127.9, 126.8, 123.9, 123.8, 122.6, 122.2, 121.5, 121.1, 119.0, 117.8, 116.3, 77.3, 77.0, 76.7, 44.7, 34.5, 33.9, 31.0, 30.5. DEPT-135 (101 MHz, Chloroform-*d*) δ 138.5, 131.4, 129.3, 128.2, 127.9, 126.8, 123.9, 123.8, 122.6, 121.5, 116.3, 77.2, 31.0, 30.5. MS (EI) m/z: 591.22 [M<sup>+</sup>]. Calcd for C<sub>40</sub>H<sub>33</sub>NO<sub>2</sub>S: 591.77

#### **Synthesis of 2,6-di-tert-butyl-12*H*-spiro[benzo[9,1]quinolizino[3,4,5,6,7-*klmn*]phenothiazine-8,9'-xanthen]-12-one 4,4-dioxide (SPA-SO2)**

A round-bottom flask equipped with a magnetic stirrer was charged with substrate SPA-S (1 g, 1.69 mmol), H<sub>2</sub>O<sub>2</sub> (229.9 mg, 6.76 mmol), and HOAc (50 mL). The mixture was refluxed for 4 hours under air. The reaction progress was monitored by TLC. After cooling to room temperature, the reaction mixture was added dropwise to an aqueous solution of sodium thiosulfate ( $\approx$ 1 M) and extracted with dichloromethane. The solvent was removed under reduced pressure, and the residue was purified by column chromatography on silica gel using petroleum ether/ethyl acetate (9/1, v/v) as the eluent, yielding a pale yellow solid. The final product was obtained with a yield of 800 mg (75%). <sup>1</sup>H NMR (400 MHz, Chloroform-*d*) δ 9.02 (d, *J* = 2.7 Hz, 1H), 8.72 (d, *J* = 2.7 Hz, 1H), 8.53 (dd, *J* = 7.7, 1.9 Hz, 1H), 8.15 (d, *J* = 2.5 Hz, 1H), 7.49 (dd, *J* = 7.6, 1.8 Hz, 1H), 7.42 – 7.30 (m, 2H), 7.25 – 7.19 (m, 4H), 6.89 (d, *J* = 8.3, 6.0, 2.4 Hz, 2H), 6.78 – 6.71 (m, 2H), 1.53 (s, 9H), 1.14 (s, 9H). <sup>13</sup>C NMR (101 MHz, Chloroform-*d*) δ 176.5, 149.6, 148.3, 148.0, 148.0, 139.3, 135.8, 134.2, 133.6, 133.3, 133.2, 131.4, 130.3, 130.2, 128.8, 128.3, 127.4, 127.0, 125.7, 124.3, 123.7, 123.4, 122.5, 122.0, 119.8, 116.6, 77.4, 77.0, 76.7, 44.4, 35.2, 34.6, 31.2, 30.6. DEPT-135 (101 MHz, Chloroform-*d*) δ 139.3, 135.8, 131.4, 130.3, 128.8, 127.4, 127.1, 125.7, 124.3, 119.8, 116.6, 77.2, 31.2, 30.6. MS (EI) m/z: 623.34 [M<sup>+</sup>]. Calcd for C<sub>40</sub>H<sub>33</sub>NO<sub>4</sub>S: 623.33



### 3. NMR spectra

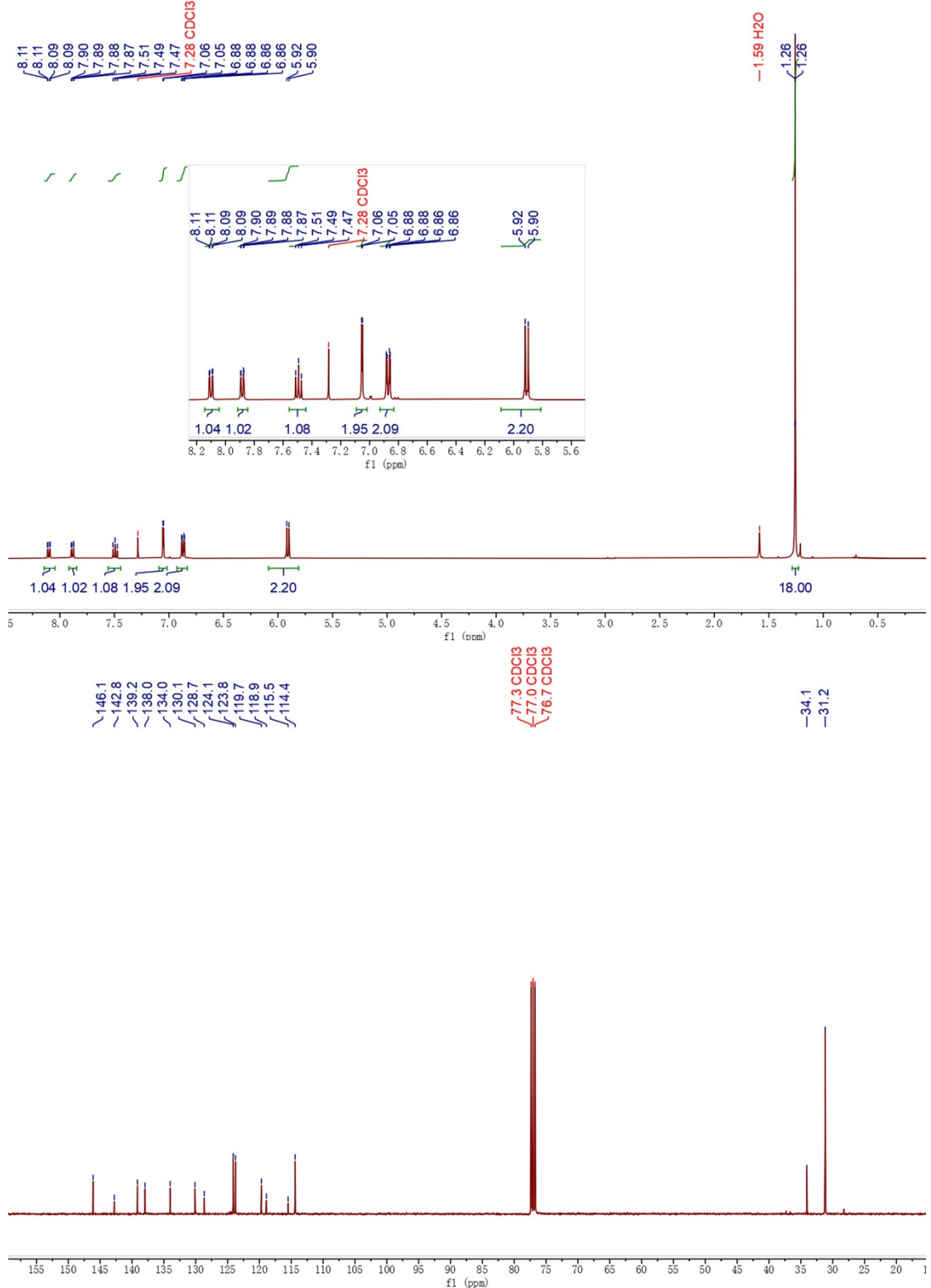


**Fig. S1.**  $^1\text{H}$  NMR (400 MHz, Chloroform-*d*) and  $^{13}\text{C}$  NMR (101 MHz, Chloroform-*d*) spectra of *3-bromo-2-(3,7-di-tert-butyl-10H-phenothiazin-10-yl)benzonitrile* (2)

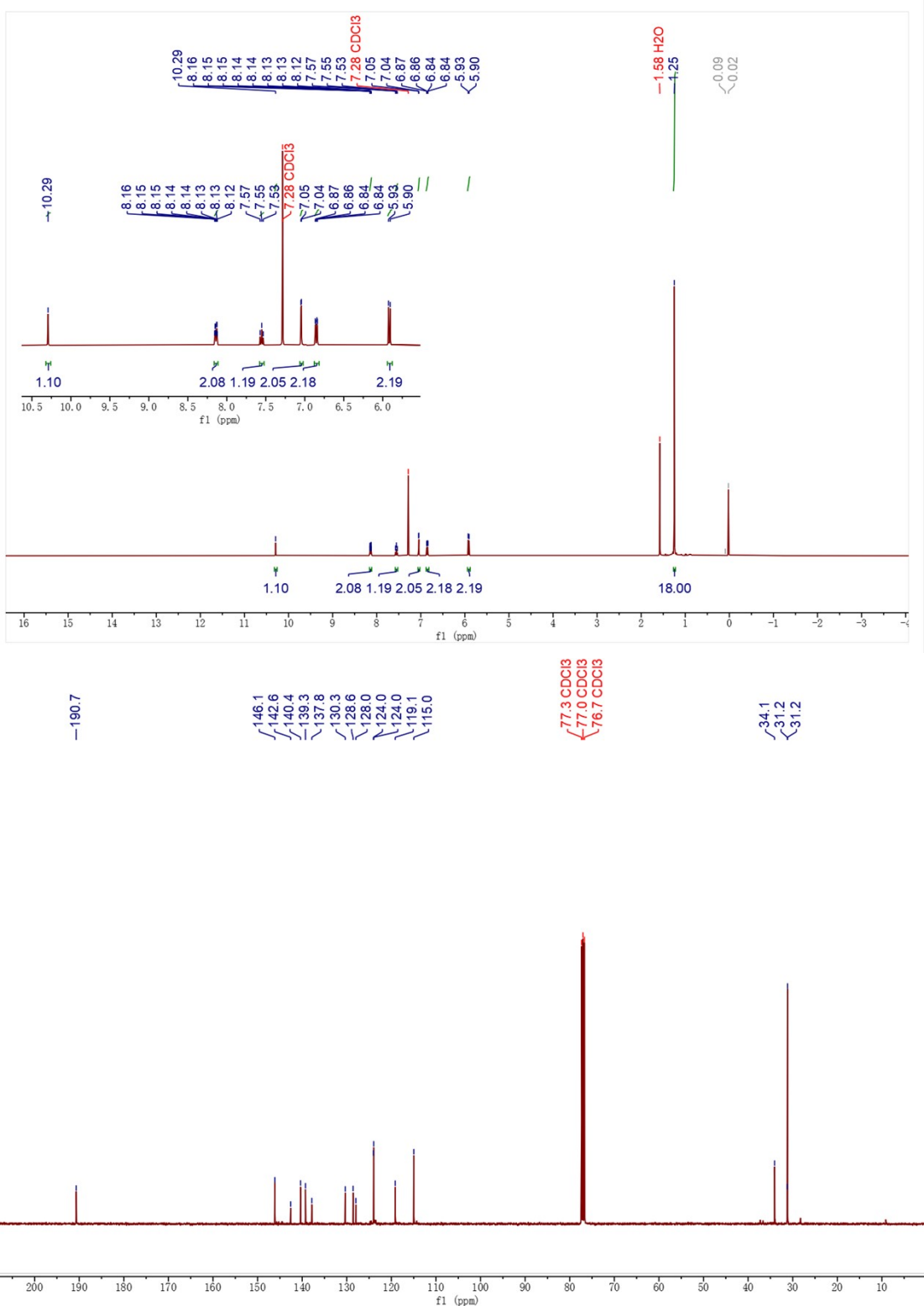


**Fig. S2.**  $^1\text{H}$  NMR (400 MHz, Chloroform-*d*) and  $^{13}\text{C}$  NMR (101 MHz, Chloroform-*d*) spectra of 3-bromo-2-(3,7-di-*tert*-butyl-10*H*-phenothiazin-10-yl)benzaldehyde (3)

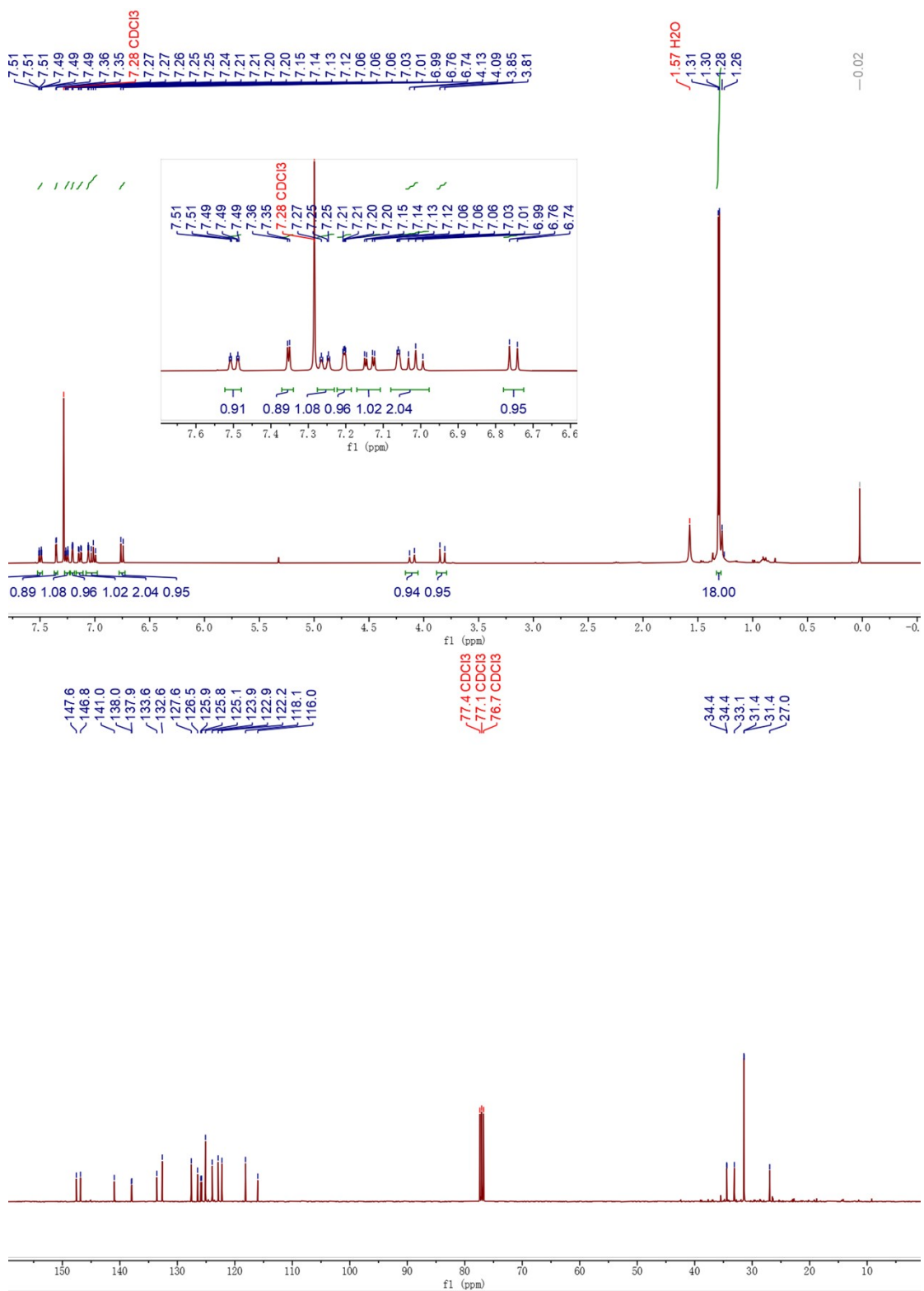


**Fig. S3.**  $^1\text{H}$  NMR (400 MHz, Chloroform-*d*) and  $^{13}\text{C}$  NMR (101 MHz, Chloroform-*d*) spectra of *13-bromo-3,7-di-tert-butyl-9H-quinolino[3,2,1-kl]phenothiazine* (4)

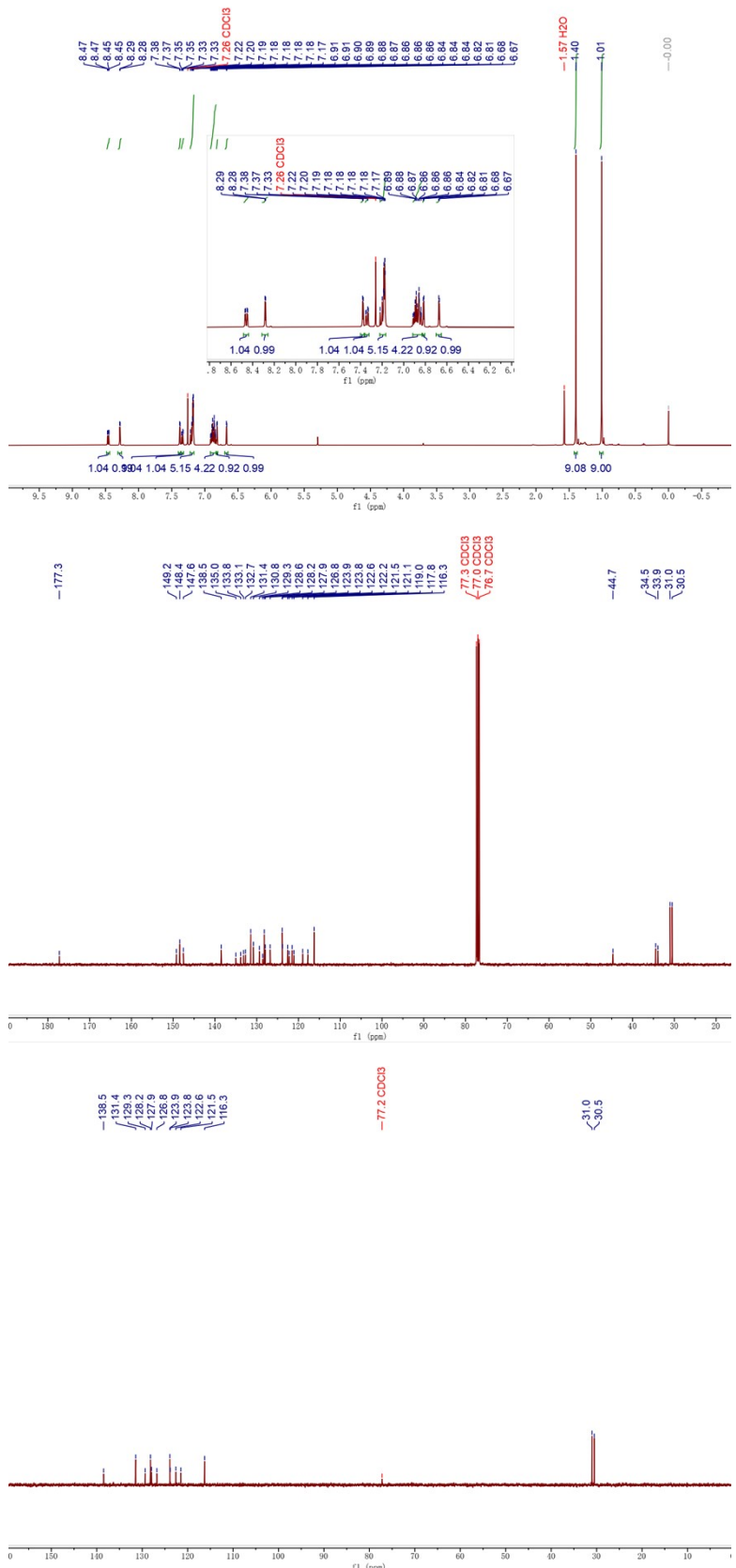


**Fig. S4.**  $^1\text{H}$  NMR (400 MHz, Chloroform-*d*),  $^{13}\text{C}$  NMR (101 MHz, Chloroform-*d*) and DEPT (101 MHz, Chloroform-*d*) spectra of SPA-S.



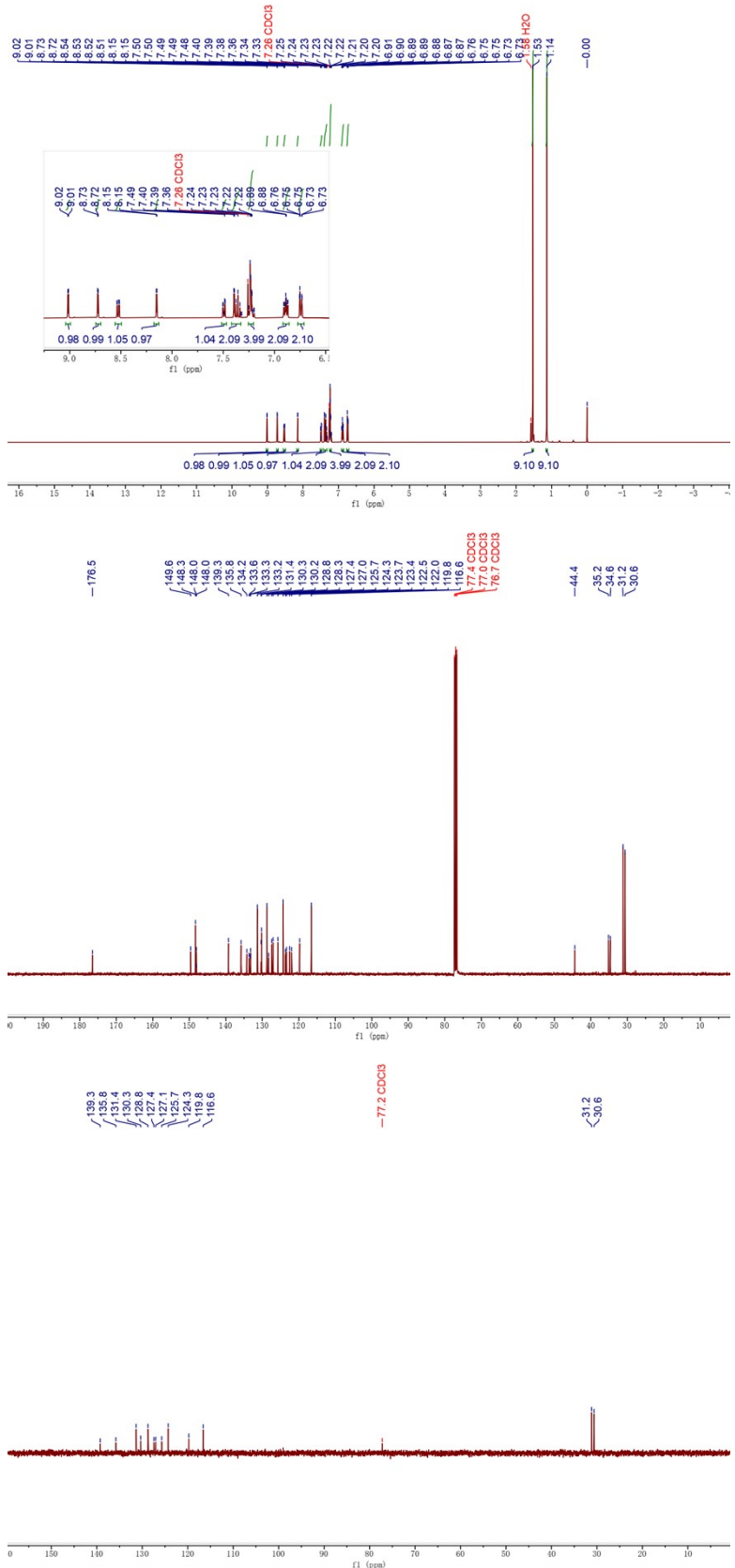


**Fig. S5.**  $^1\text{H}$  NMR (400 MHz, Chloroform-*d*),  $^{13}\text{C}$  NMR (101 MHz, Chloroform-*d*) and DEPT-135 (101 MHz, Chloroform-*d*) spectra of SPA-SO<sub>2</sub>.

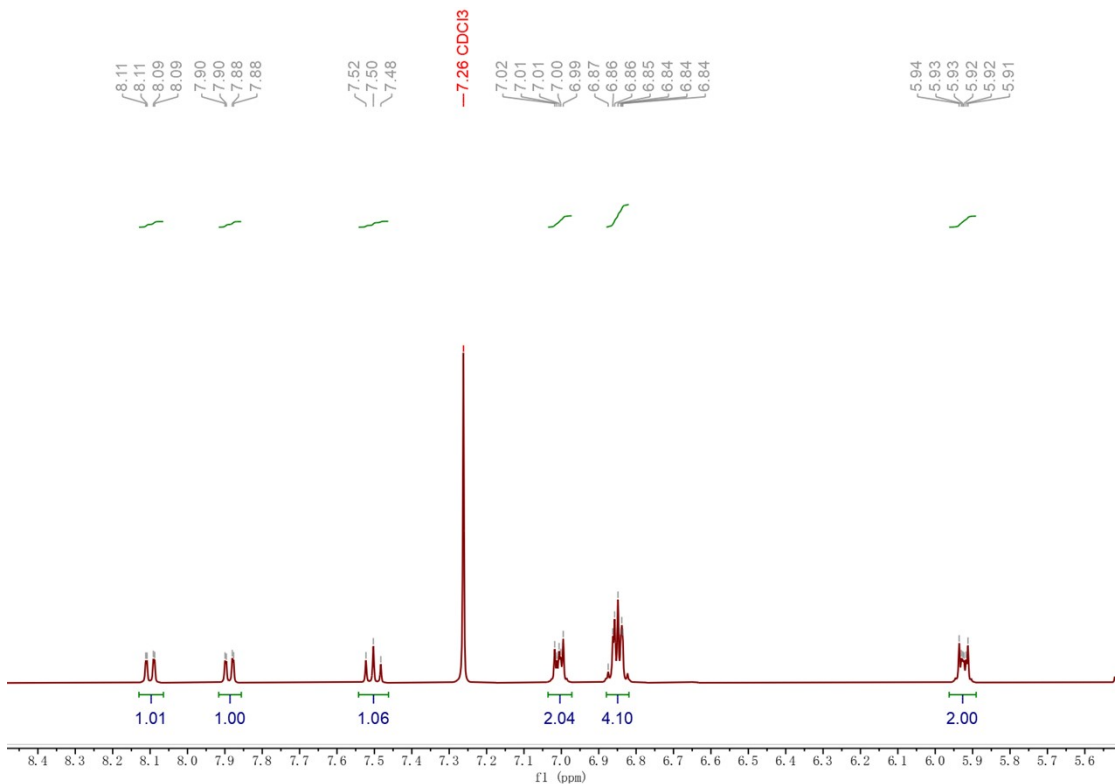
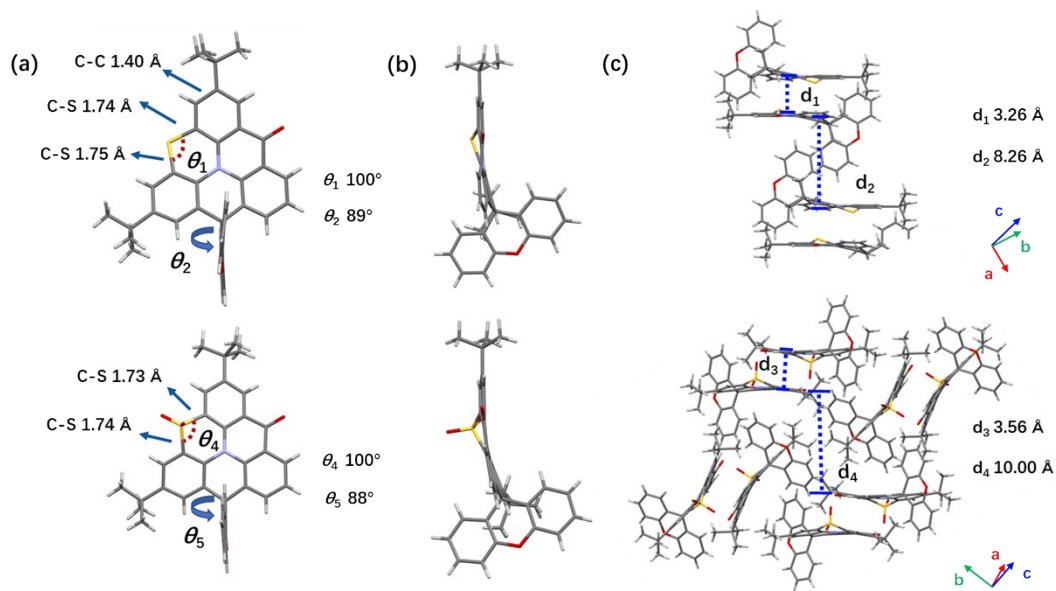


**Figure S6.** The aromatic region of the  $^1\text{H}$  NMR (400 MHz, Chloroform-*d*) spectra of compound 5.

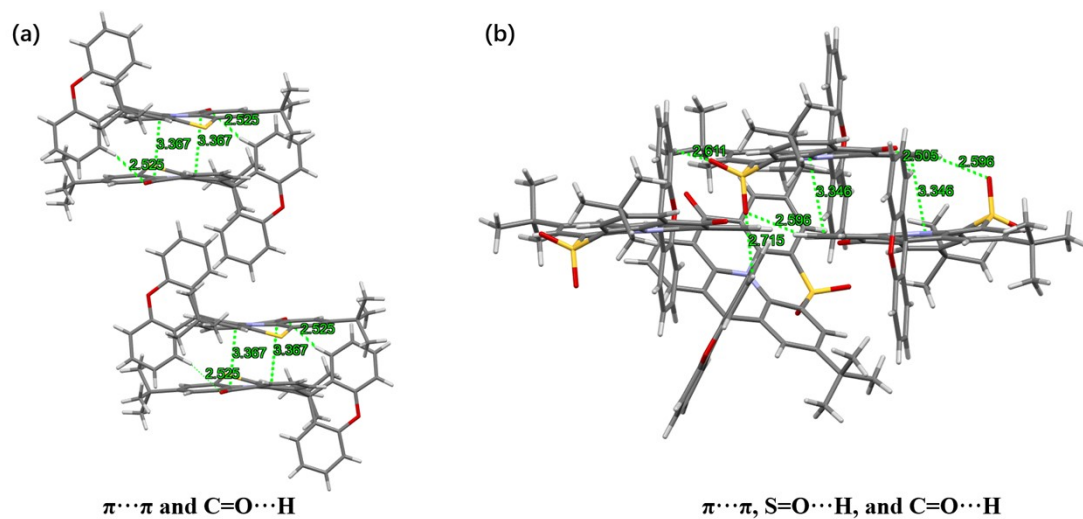
## 4. Crystal

**Table S1**

Identification code	SPA-S	SPA-SO2
Empirical formula	C <sub>40</sub> H <sub>33</sub> NO <sub>2</sub> S	C <sub>40</sub> H <sub>33</sub> NO <sub>4</sub> S
Formula weight	591.73	623.73
Temperature/K	296	298
Crystal system	monoclinic	monoclinic
Space group	P2 <sub>1</sub> /c	P2 <sub>1</sub> /n
a/Å	12.1764(9)	12.3448(13)
b/Å	15.4723(12)	14.6938(17)
c/Å	17.0863(13)	18.8307(18)
α/°	90	90
β/°	103.779(2)	106.577(3)
γ/°	90	90
Volume/Å <sup>3</sup>	3126.4(4)	3273.8(6)
Z	4	4
ρ <sub>calc</sub> g/cm <sup>3</sup>	1.257	1.265
μ/mm <sup>-1</sup>	0.14	0.142
F(000)	1248	1312
Crystal size/mm <sup>3</sup>	0.12 × 0.06 × 0.04	0.15 × 0.06 × 0.04
Radiation	MoKα ( $\lambda = 0.71073$ )	MoKα ( $\lambda = 0.71073$ )
2θ range for data collection/°	4.336 to 55.008	4.42 to 52.778
Index ranges	-15 ≤ h ≤ 15, -19 ≤ k ≤ 20, -22 ≤ l ≤ 18	-13 ≤ h ≤ 15, -17 ≤ k ≤ 18, -23 ≤ l ≤ 23
Reflections collected	20844	22976
Independent reflections	6991 [R <sub>int</sub> = 0.0854, R <sub>sigma</sub> = 0.1056]	6665 [R <sub>int</sub> = 0.0922, R <sub>sigma</sub> = 0.0990]
Data/restraints/parameters	6991/36/403	6665/36/421
Goodness-of-fit on F <sup>2</sup>	1.021	1.035
Final R indexes [I>=2σ (I)]	R <sub>1</sub> = 0.0816, wR <sub>2</sub> = 0.1967	R <sub>1</sub> = 0.1000, wR <sub>2</sub> = 0.2027
Final R indexes [all data]	R <sub>1</sub> = 0.1690, wR <sub>2</sub> = 0.2518	R <sub>1</sub> = 0.1863, wR <sub>2</sub> = 0.2543
Largest diff. peak/hole / e Å <sup>-3</sup>	0.66/-0.34	0.66/-0.47

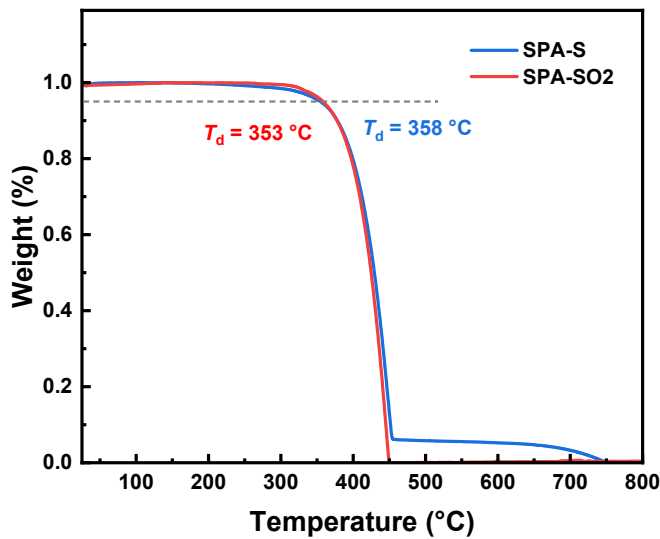


**Fig. S7.** (a) Top and (b) side view, along with (c) packing mode of the single-crystal structures of (top) SPA-S and (bottom) SPA-SO2.

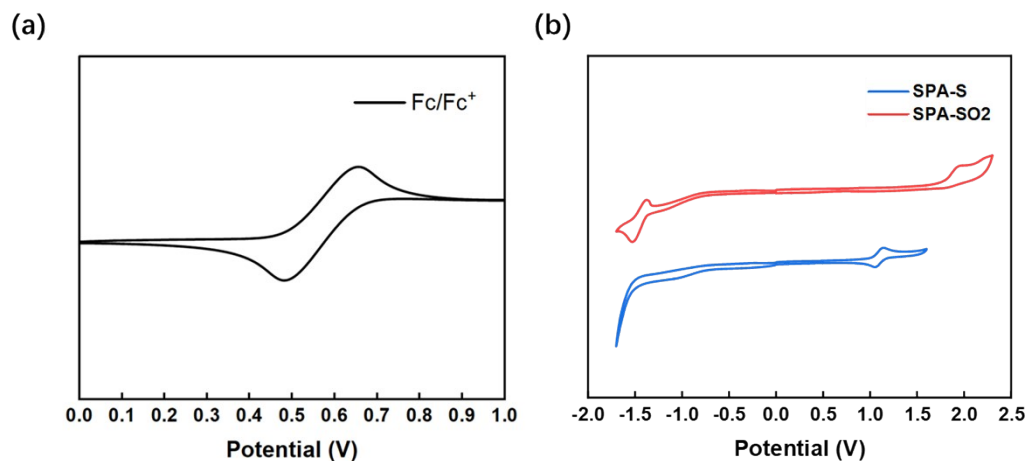


**Fig. S8.** Intermolecular and intramolecular interactions for (a) SPA-S and (b) SPA-SO2.

## 5. Thermal and electrochemical properties

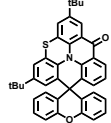
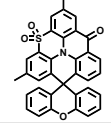
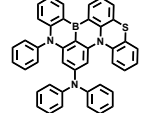
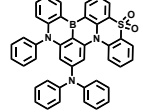
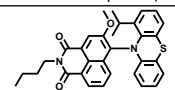
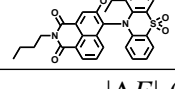
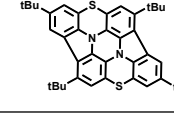
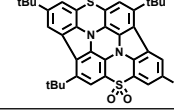
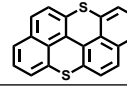
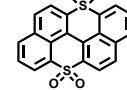


**Fig. S9.** TGA curves of SPA-S and SPA-SO2.



**Fig. S10.** CV curve of (a) ferrocene, (b) SPA-S, and SPA-SO2.

**Table S2.** Data from literature reporting the same oxidation phenomenon, HOMO, LUMO,  $E_g$  levels, and absolute energy difference of the reactant and product.

DOI	Structure	Name	$E_{\text{HOMO}}$ (eV)	$E_{\text{LUMO}}$ (eV)	$E_g$ (eV)
This work		SPA-S	-5.25	-2.70	2.55
		SPA-SO2	-6.00	-2.88	3.12
	$ \Delta E $ (eV)		0.75	0.18	0.57
10.1002/adfm. 202201032		PTZBN2	-5.13	-2.52	2.61
		PTZBN3	-5.35	-2.69	2.66
	$ \Delta E $ (eV)		0.22	0.17	0.05
10.31635/ccschem. 023.202303152		MINI-PTZ1	-5.89	-3.11	2.78
		MINI-PTZ2	-6.54	-3.23	3.31
	$ \Delta E $ (eV)		0.65	0.12	0.53
10.1002/anie. 202218892		tPT	-5.06	-2.39	2.67
		tPD	-5.85	-3.25	2.60
	$ \Delta E $ (eV)		0.79	0.86	0.07
10.1002/anie. 202211412		PTT	-4.88	-2.49	2.39
		PTT-O4	-5.13	-2.18	2.95
	$ \Delta E $ (eV)		0.25	0.31	0.56

## 6. Photophysical properties

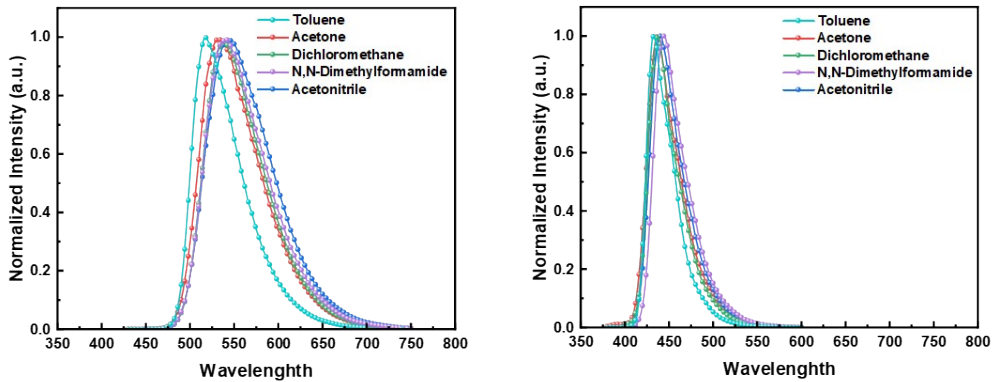


**Fig. S11.** Fluorescence spectra of (left) SPA-S and (right) SPA-SO2 in various solvents (toluene, acetone, acetonitrile, dichloromethane, and *N,N*-Dimethylformamide).

**Table S3.** Photophysical properties of SPA-S and SPA-SO2 in various solvents.

	SPA-S		SPA-SO2	
	$\lambda_{PL}$	FWHM	$\lambda_{PL}$	FWHM
	nm	nm	nm	nm
Toluene	517	60	433	33
Acetone	530	75	437	39
Dichloromethane	537	75	437	36
<i>N,N</i> -Dimethylformamide	542	78	444	39
Acetonitrile	544	84	439	40

## 7. Theoretical calculations

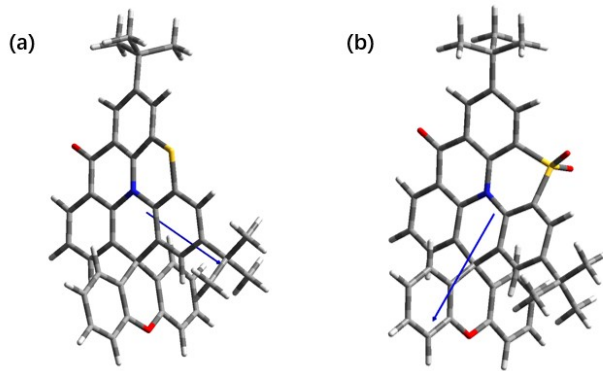


**Fig. S12.** Dipole Moment of (a) SPA-S and (b) SPA-SO<sub>2</sub>, SPA-S dipole moment is carbonyl pointing to nitrogen atom, SPA-SO<sub>2</sub> dipole moment is nitrogen atom pointing to oxygen atom.

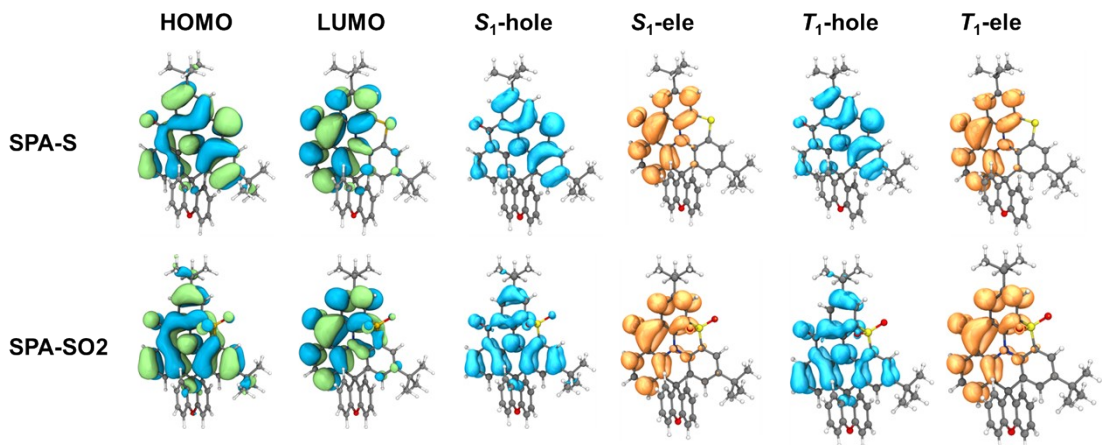


**Fig. S13.** Frontier molecular orbitals and excited state electron-hole distribution from DFT/TD-DFT simulations of SPA-S and SPA-SO<sub>2</sub>.

**Table S4.** Calculated excitation states for the first five singlet states of two molecules, with oscillator strengths (f), electron-hole center distances (D\_idx), electron-hole overlap integrals (Sr), and orbital composition (orb) for each state.

	sn	Mult	E (eV)	E (nm)	f	D_idx	Sr	orb
SPA-S	1	Singlet	2.83	437.85	0.160	2.464	0.608	H-L:0.982
	2	Singlet	3.36	368.82	0.003	0.963	0.661	H-L2:0.72; H-L1:0.248
	3	Singlet	3.51	353.19	0.071	2.691	0.545	H-L1:0.723; H-L2:0.246
	4	Singlet	3.60	344.74	0.000	0.895	0.413	H4-L:0.701; H1-L:0.262
	5	Singlet	3.68	337.14	0.001	4.277	0.284	H1-L:0.725;

									H4-L:0.247
<b>SPA-SO2</b>	1	Singlet	3.21	385.78	0.178	1.823	0.623	H-L:0.971	
	2	Singlet	3.40	364.93	0.000	5.810	0.185	H1-L:0.938; H3-L:0.038	
	3	Singlet	3.56	348.45	0.001	1.377	0.429	H3-L:0.564; H5-L:0.251	
	4	Singlet	3.95	313.77	0.036	0.963	0.706	H-L1:0.793; H2-L:0.145	
	5	Singlet	3.99	310.98	0.022	3.434	0.625	H2-L:0.755; H-L1:0.148	

**Table S5.** Calculated excitation states for the first five triplet states of two molecules, with electron-hole center distances (D\_idx), electron-hole overlap integrals (Sr), and orbital composition (orb) for each state.

	sn	Mult	E (eV)	E (nm)	D_idx	Sr	orb
<b>SPA-S</b>	1	Triplet	2.32	534.81	2.464	0.585	H-L:0.945
	2	Triplet	2.75	450.24	0.348	0.643	H-L2:0.545; H-L1:0.172
	3	Triplet	3.08	402.72	1.288	0.611	H-L1:0.321; H-L2:0.235
	4	Triplet	3.10	399.75	1.926	0.590	H2-L:0.414; H-L5:0.118
	5	Triplet	3.22	384.76	1.619	0.409	H4-L:0.909
<b>SPA-SO2</b>	1	Triplet	2.66	466.91	1.279	0.636	H-L:0.915; H9-L:0.029
	2	Triplet	3.13	395.87	0.895	0.670	H4-L:0.184; H-L2:0.176
	3	Triplet	3.14	394.36	1.576	0.412	H3-L:0.547; H5-L:0.242
	4	Triplet	3.21	386.37	1.132	0.594	H-L3:0.347; H7-L:0.235
	5	Triplet	3.36	369.47	0.452	0.645	H-L2:0.226; H9-L:0.115

**Table S6.** Calculated spin-orbit coupling (SOC) constants ( $\text{cm}^{-1}$ ) for the singlet and triplet states of molecules SPA-S and SPA-SO2.

		$S_0$	$S_1$	$S_2$
SPA-S	$T_1$	3.97	0.34	3.63
	$T_2$	19.03	1.29	0.18
	$T_3$	4.69	0.85	1.02
SPA-	$T_1$	1.60	0.71	5.94

SO2	$T_2$	2.65	1.49	3.99
	$T_3$	42.57	10.52	0.58

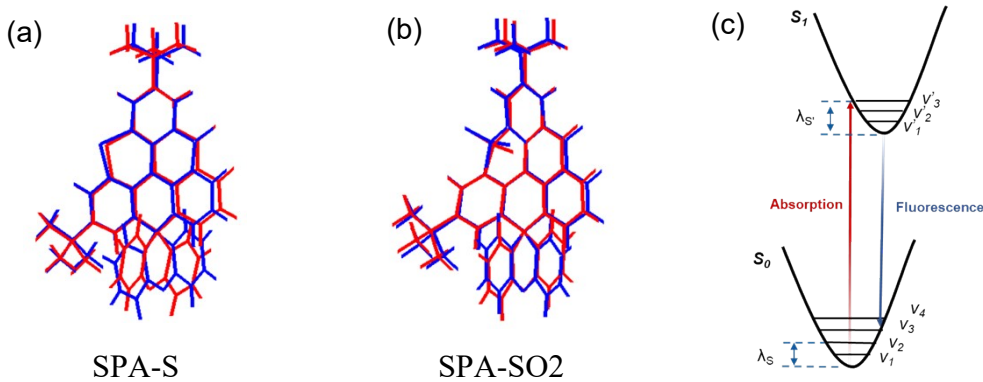


**Fig. S14.** The geometric difference between the  $S_0$  (blue) and  $S_1$  (red) configurations for (a) SPA-S and SPA-SO2; (c) Potential energy surfaces in the ground and the excited states.

**Table S7.** The root means square displacement/deviation (RMSD) values, reorganization energy and Simulation of Stokes shifts for SPA-S and SPA-SO2.

	SPA-S	SPA-SO2
<b>RMSD</b>	0.415	0.378
$\lambda_{S'}$ (eV)	0.258	0.121
$\lambda_S$ (eV)	0.200	0.147
$\lambda_{S'} + \lambda_S$ (eV)	0.458	0.268
$\lambda_{\text{Stokes}}$ (nm)	89	40

Modelling Stokes shift using calculated recombination energies and absorption wavelengths

$$\lambda_{\text{Stokes}} = \frac{1240}{\frac{1240}{\lambda_{\text{abs}}} - E_\lambda} - \lambda_{\text{abs.}} \quad (1)$$

Where  $\lambda_{\text{Stokes}}$  is stokes shift,  $\lambda_{\text{abs}}$  is absorption wavelengths,  $E_\lambda$  is recombination energies between  $S_0$  and  $S_1$ .

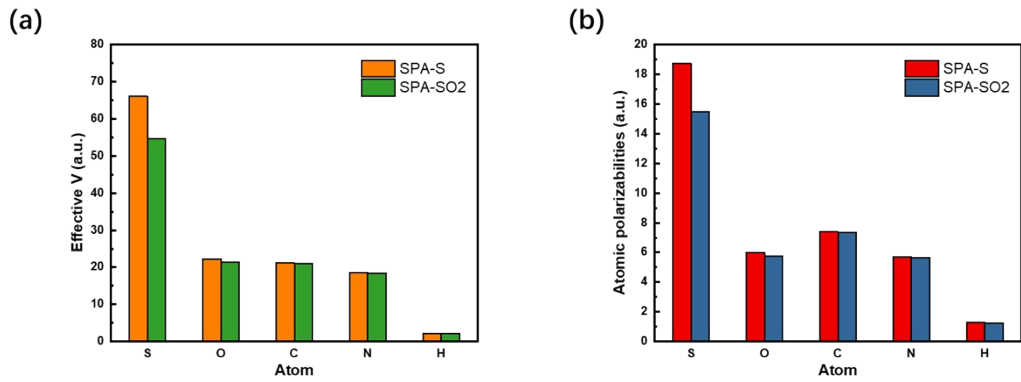


**Fig. S15.** Calculation of the effective volume of atoms within a molecule (a), and estimation of the average atomic polarizability contribution using the Tkatchenko-Scheffler (TS) method (b).

**Table S8.** Free volume and polarizability of reference data atoms in an isolated state.

Free V		Ref. data of Atomic polarizabilities	
Units	a.u.	a.u.	a.u.
S	68.40		19.40
O	19.66		5.30
C	32.35		11.30
N	24.04		7.40
H	7.38		4.51

**Table S9.** Data of calculation of the average effective volume of atoms within a molecule, and estimation of the atomic polarizability contribution using the Tkatchenko-Scheffler (TS) method.

SPA-S	Effective V	Atomic polarizabilities estimated	SPA-SO2	Effective V	Atomic polarizabilities estimated
Units	a.u.	a.u.	Atom 1(S)	Atom 1(S)	a.u.
Atom 1(S)	66.08	18.74	Atom 1(S)	54.659	15.50
Atom 2(O)	23.46	6.32	Atom 2(O)	21.318	5.75
Atom 3(N)	18.50	5.69	Atom 3(O)	19.764	5.33
Atom 4(O)	21.01	5.66	Atom 4(O)	23.25	6.27
Atom 5(C)	19.11	6.67	Atom 5(N)	18.314	5.64
Atom 6(C)	19.29	6.74	Atom 6(O)	20.953	5.65
Atom 7(C)	17.99	6.28	Atom 7(C)	19.13	6.68
Atom 8(C)	19.62	6.85	Atom 8(C)	18.394	6.42
Atom 9(C)	19.21	6.71	Atom 9(C)	17.696	6.18
Atom 10(C)	19.49	6.81	Atom 10(C)	18.998	6.64
Atom 11(C)	16.54	5.78	Atom 11(C)	17.248	6.02

Atom 12(C)	19.99	6.98	Atom 12(C)	19.117	6.68
Atom 13(C)	18.68	6.52	Atom 13(C)	19.904	6.95
Atom 14(C)	21.52	7.52	Atom 14(C)	19.626	6.85
Atom 15(H)	1.70	1.04	Atom 15(C)	21.436	7.49
Atom 16(C)	23.11	8.07	Atom 16(H)	1.693	1.03
Atom 17(H)	1.24	0.76	Atom 17(C)	21.611	7.55
Atom 18(C)	21.91	7.65	Atom 18(H)	1.444	0.88
Atom 19(H)	1.54	0.94	Atom 19(C)	18.065	6.31
Atom 20(C)	17.35	6.06	Atom 20(C)	22.549	7.88
Atom 21(C)	18.77	6.56	Atom 21(H)	1.505	0.92
Atom 22(C)	19.92	6.96	Atom 22(C)	18.114	6.33
Atom 23(C)	22.19	7.75	Atom 23(C)	20.847	7.28
Atom 24(H)	2.24	1.37	Atom 24(C)	21.224	7.41
Atom 25(C)	18.74	6.54	Atom 25(C)	21.629	7.55
Atom 26(C)	22.41	7.83	Atom 26(H)	1.458	0.89
Atom 27(H)	1.45	0.89	Atom 27(C)	16.549	5.78
Atom 28(C)	20.97	7.33	Atom 28(C)	19.967	6.97
Atom 29(C)	21.42	7.48	Atom 29(C)	19.541	6.83
Atom 30(C)	19.37	6.77	Atom 30(C)	22.923	8.01
Atom 31(C)	22.51	7.86	Atom 31(H)	1.254	0.77
Atom 32(H)	1.88	1.15	Atom 32(C)	21.852	7.63
Atom 33(C)	22.19	7.75	Atom 33(H)	1.505	0.92
Atom 34(H)	1.63	0.99	Atom 34(C)	21.031	7.35
Atom 35(C)	19.43	6.79	Atom 35(C)	22.077	7.71
Atom 36(C)	22.00	7.68	Atom 36(H)	2.208	1.35
Atom 37(H)	1.81	1.10	Atom 37(C)	19.372	6.77
Atom 38(C)	22.21	7.76	Atom 38(C)	22.211	7.76
Atom 39(H)	1.60	0.98	Atom 39(H)	1.561	0.95
Atom 40(C)	20.87	7.29	Atom 40(C)	22.147	7.74
Atom 41(C)	21.92	7.66	Atom 41(H)	1.634	1.00
Atom 42(H)	2.02	1.23	Atom 42(C)	20.838	7.28
Atom 43(C)	21.09	7.37	Atom 43(C)	22.006	7.69
Atom 44(C)	22.56	7.88	Atom 44(H)	2.005	1.23
Atom 45(H)	2.26	1.38	Atom 45(C)	19.308	6.74
Atom 46(C)	22.68	7.92	Atom 46(C)	22.605	7.90
Atom 47(H)	2.23	1.36	Atom 47(H)	2.221	1.36
Atom 48(C)	22.56	7.88	Atom 48(C)	22.523	7.87
Atom 49(H)	2.26	1.38	Atom 49(H)	2.249	1.37
Atom 50(C)	22.65	7.91	Atom 50(C)	22.62	7.90
Atom 51(H)	2.23	1.36	Atom 51(H)	2.221	1.36
Atom 52(C)	22.03	7.69	Atom 52(C)	22.499	7.86

Atom 53(H)	2.02	1.23	Atom 53(H)	2.239	1.37
Atom 54(C)	24.35	8.51	Atom 54(C)	21.989	7.68
Atom 55(H)	2.18	1.33	Atom 55(H)	2.008	1.23
Atom 56(H)	2.35	1.43	Atom 56(C)	24.187	8.45
Atom 57(H)	2.19	1.34	Atom 57(H)	2.165	1.32
Atom 58(C)	24.21	8.45	Atom 58(H)	2.328	1.42
Atom 59(H)	2.17	1.33	Atom 59(H)	2.168	1.33
Atom 60(H)	2.35	1.44	Atom 60(C)	23.742	8.29
Atom 61(H)	2.17	1.33	Atom 61(H)	2.22	1.36
Atom 62(C)	23.86	8.33	Atom 62(H)	2.341	1.43
Atom 63(H)	2.23	1.36	Atom 63(H)	2.14	1.31
Atom 64(H)	2.36	1.44	Atom 64(C)	23.738	8.29
Atom 65(H)	2.17	1.33	Atom 65(H)	2.134	1.30
Atom 66(C)	23.83	8.32	Atom 66(H)	2.342	1.43
Atom 67(H)	2.16	1.32	Atom 67(H)	2.232	1.36
Atom 68(H)	2.36	1.44	Atom 68(C)	23.592	8.24
Atom 69(H)	2.23	1.36	Atom 69(H)	2.255	1.38
Atom 70(C)	23.63	8.25	Atom 70(H)	2.346	1.43
Atom 71(H)	2.28	1.39	Atom 71(H)	2.127	1.30
Atom 72(H)	2.36	1.44	Atom 72(C)	24.17	8.44
Atom 73(H)	2.12	1.30	Atom 73(H)	2.167	1.32
Atom 74(C)	23.59	8.24	Atom 74(H)	2.332	1.43
Atom 75(H)	2.17	1.33	Atom 75(H)	2.164	1.32
Atom 76(H)	2.36	1.44	Atom 76(C)	23.558	8.23
Atom 77(H)	2.26	1.38	Atom 77(H)	2.174	1.33
			Atom 78(H)	2.344	1.43
			Atom 79(H)	2.253	1.38

**Table S10.** Data of molecular coordinates

Cartesian coordinates of optimized SPA-S				Cartesian coordinates of optimized SPA-SO2			
Atom	X	Y	Z	Atom	X	Y	Z
S	-2.05206	2.620313	-0.73835	S	2.017086	2.281154	-0.82147
O	-3.70437	-3.50816	-0.21161	O	2.539821	3.525894	-0.23559
N	-1.01627	-0.3474	-0.31755	O	1.940068	2.168544	-2.28785
O	4.79379	-1.14395	0.475036	O	3.410286	-3.82203	0.031938
C	-0.55171	-1.67748	-0.33626	N	0.881055	-0.5404	-0.21245
C	-3.33457	-1.17173	-0.1349	O	-5.01523	-1.19584	0.018409
C	-2.40889	-0.10961	-0.24957	C	3.153439	-1.46934	0.013324
C	-1.46187	-2.76943	-0.37683	C	-0.01142	0.565606	-0.11863
C	1.312967	0.463123	-0.06844	C	2.274931	-0.36962	-0.15156

C	2.52048	-1.19008	1.33016	C	0.34713	-1.8545	-0.2037
C	1.90059	-0.94306	-0.05005	C	2.661107	-2.85396	-0.04452
C	0.827623	-1.98661	-0.30171	C	-1.39355	0.385931	0.074489
C	-0.05876	0.721678	-0.23715	C	-1.04395	-2.0838	-0.19267
C	-1.00366	-4.09197	-0.48345	C	1.205088	-2.98606	-0.19621
H	-1.76415	-4.87298	-0.51493	C	0.682574	-4.28555	-0.27177
C	2.227615	1.511755	0.067759	H	1.400109	-5.10674	-0.26556
H	3.275877	1.247066	0.200602	C	4.275824	1.069224	-0.01728
C	1.247717	-3.31159	-0.41227	H	4.651895	2.090473	-0.06725
H	2.321129	-3.50906	-0.39031	C	2.908001	0.891501	-0.21533
C	-2.90782	-2.57216	-0.23966	C	4.529586	-1.27584	0.189197
C	-0.42964	2.08259	-0.31617	H	5.116185	-2.18782	0.307259
C	2.97876	-1.02939	-1.13348	C	0.427324	1.906281	-0.16746
C	0.350232	-4.37453	-0.52636	C	-1.7604	2.809863	0.352265
H	0.712291	-5.40022	-0.61623	C	5.128457	-0.01567	0.216307
C	-2.97755	1.190194	-0.29432	C	-0.40551	2.997463	0.079232
C	-4.71677	-0.94276	0.018485	H	0.043758	3.988514	0.034954
H	-5.33004	-1.83811	0.095008	C	-2.07215	-0.97248	-0.04243
C	1.860015	2.855017	0.041696	C	-2.90302	-1.22907	1.216938
C	-5.25418	0.332374	0.061968	C	-2.97608	-0.93929	-1.27785
C	3.905899	-1.25502	1.510163	C	-2.21674	1.488638	0.306226
C	-4.34165	1.390907	-0.11031	H	-3.27763	1.288257	0.456783
H	-4.70036	2.422277	-0.12674	C	-1.52969	-3.39013	-0.27558
C	2.62208	-0.98672	-2.48914	H	-2.61188	-3.53321	-0.27921
H	1.562641	-0.92564	-2.7481	C	6.634766	0.134134	0.454464
C	4.337656	-1.10554	-0.81361	C	-0.68479	-4.4979	-0.33583
C	0.502346	3.113396	-0.1588	H	-1.09662	-5.50615	-0.40519
H	0.130846	4.136508	-0.209	C	-4.29799	-1.31387	1.175567
C	1.702868	-1.31199	2.46336	C	-2.41646	-0.77614	-2.55391
H	0.619102	-1.26559	2.335727	H	-1.33111	-0.69066	-2.64504
C	2.917605	3.951244	0.211675	C	-2.26994	-1.35661	2.462272
C	4.465209	-1.43201	2.783067	H	-1.18023	-1.29167	2.503979
H	5.552074	-1.47829	2.870515	C	-2.73312	3.954838	0.649389
C	-6.74561	0.623134	0.25928	C	-5.04585	-1.52051	2.343892
C	3.583634	-1.01537	-3.49532	H	-6.13233	-1.57967	2.260492
H	3.280003	-0.97889	-4.54339	C	-4.36698	-1.04024	-1.17571
C	3.634241	-1.54555	3.893065	C	-4.39633	-1.64293	3.567558
H	4.071394	-1.68368	4.884454	H	-4.98057	-1.80336	4.476297
C	2.242879	-1.48691	3.73466	C	-2.998	-1.56105	3.63054
H	1.584105	-1.57766	4.600525	H	-2.48168	-1.65648	4.587656
C	4.94112	-1.08854	-3.15276	C	-4.60553	-0.82005	-3.56982

H	5.706108	-1.11174	-3.93204	H	-5.24255	-0.77409	-4.45583
C	5.318804	-1.13558	-1.81477	C	-3.21294	-0.71584	-3.69363
H	6.365968	-1.19715	-1.51369	H	-2.75331	-0.58601	-4.6752
C	2.30235	5.357015	0.149504	C	-5.18246	-0.98282	-2.31466
H	1.560107	5.513196	0.947554	H	-6.26259	-1.06817	-2.18434
H	3.091263	6.114112	0.275659	C	7.070475	1.606507	0.431639
H	1.812623	5.545687	-0.81835	H	6.562612	2.195388	1.211058
C	-7.5562	-0.67014	0.428506	H	8.153354	1.675567	0.615158
H	-7.22138	-1.24894	1.302708	H	6.868098	2.07777	-0.54239
H	-8.6193	-0.42524	0.574962	C	7.397758	-0.62651	-0.65012
H	-7.48076	-1.31712	-0.45852	H	7.158922	-0.21834	-1.64448
C	-7.28457	1.384066	-0.97034	H	8.484306	-0.53581	-0.49322
H	-7.16118	0.785457	-1.88626	H	7.147634	-1.69797	-0.65432
H	-8.35718	1.602287	-0.84441	C	6.9848	-0.46569	1.832356
H	-6.76457	2.342426	-1.12014	H	6.72105	-1.53242	1.889868
C	-6.9288	1.489175	1.523084	H	8.065924	-0.3755	2.023778
H	-6.39585	2.448783	1.442279	H	6.448761	0.060514	2.637653
H	-7.99604	1.71178	1.682791	C	-3.38356	3.715118	2.028311
H	-6.5499	0.966195	2.414986	H	-2.62121	3.688717	2.822427
C	3.962776	3.819532	-0.91637	H	-4.09308	4.525248	2.260054
H	3.48969	3.933128	-1.90417	H	-3.93746	2.764704	2.060619
H	4.736129	4.597586	-0.8134	C	-2.01868	5.313807	0.669814
H	4.465288	2.841003	-0.89526	H	-1.56202	5.549785	-0.30345
C	3.60931	3.775399	1.580087	H	-2.74194	6.110862	0.89937
H	4.099807	2.794292	1.666418	H	-1.22981	5.346958	1.436926
H	4.379718	4.55035	1.721326	C	-3.82498	3.983819	-0.44126
H	2.880788	3.860681	2.401384	H	-4.39342	3.042219	-0.47772
				H	-4.53874	4.799219	-0.24328
				H	-3.38175	4.148067	-1.43562

## 8. Electroluminescence properties

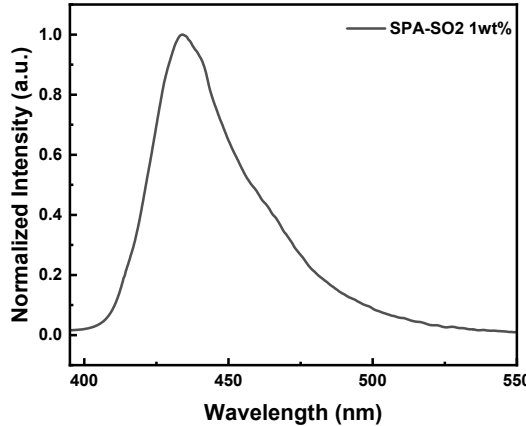


**Fig. S16.** PL spectra of SPA-SO2 in doped PPF films.

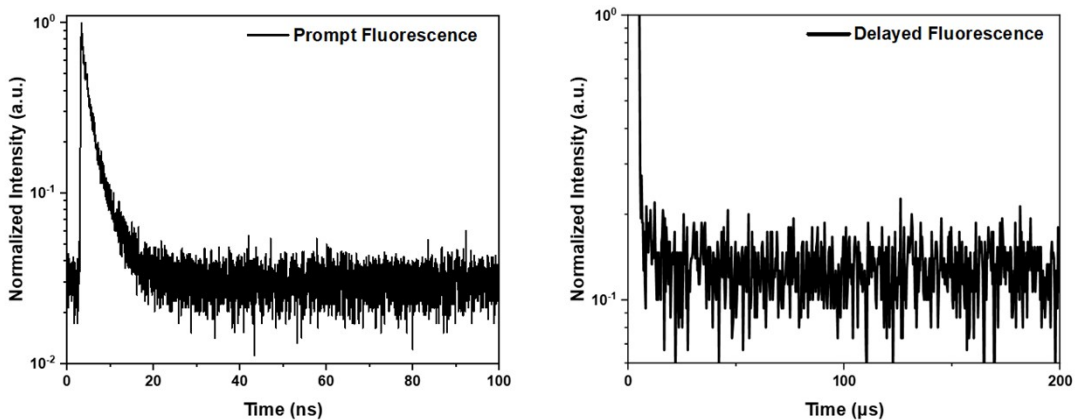


**Fig. S17.** Time-dependent transient PL spectra. The prompt decay properties of SPA-SO2.

**Table S11.** Photophysical properties of SPA-SO2 in doped PPF films.

	$\Phi_{PF}/\Phi_{DF}$	$\tau_{PF}/\tau_{DF}$	$k_p$	$k_d$	$k_{S\ r}$	$k_{S\ nr}$	$k_{ISC}$	$k_{RISC}$
	%/%	ns/μs	$\times 10^8\ s^{-1}$	$\times 10^4\ s^{-1}$	$\times 10^8\ s^{-1}$	$\times 10^8\ s^{-1}$	$\times 10^8\ s^{-1}$	$\times 10^4\ s^{-1}$
SPA-SO2	31.5/26.5	1.57/19.5	6.37	8.37	2.00	1.45	2.91	1.54

In this work, the doped films of SPA-SO2 do not exhibit phosphorescence emission at 300 K. In other words, the efficiency of phosphorescence is zero ( $\Phi_{Phos} = 0$ ). Thus, the quantum efficiency of delayed emission ( $\Phi_{DE}$ ) is equal to the efficiency of delayed fluorescence ( $\Phi_{DF}$ ). Thus, the quantum efficiencies of prompt ( $\Phi_{PF}$ ) and delayed emission ( $\Phi_{DF}$ ) are evaluated by the corrected estimation method, and the rate constants were calculated according to the reported method. [8]

$$k_{PF} = \frac{1}{\tau_{PF}}$$

$$k_{DF} = \frac{1}{\tau_{DF}}$$

$$k_r^S = k_{PF}\Phi_{PF}$$

$$k_{nr}^S = k_{PF}\frac{\Phi_{PF}}{\Phi_{all}}(1 - \Phi_{all})$$

$$k_{ISC} = k_{PF}\frac{\Phi_{DF}}{\Phi_{all}} - k_{DF}\frac{\Phi_{DF}}{\Phi_{PF}}$$

$$k_{RISC} = k_{DF}\frac{\Phi_{all}}{\Phi_{PF}}$$

$$k_{nr}^T = 0$$

where  $k_{PF}$  and  $k_{DF}$  are the radiative decay rate for prompt and delayed fluorescence, respectively;  $\Phi_{all}$  is the total photoluminescence quantum efficiency;  $k_r^S$  and  $k_{nr}^S$  are the radiative and nonradiative decay rate constants from a singlet excited state, respectively;  $k_{ISC}$  and  $k_{RISC}$  are the intersystem crossing and reverse intersystem crossing rate constants, respectively;  $k_{nr}^T$  is the nonradiative decay rate constant from a triplet excited state.

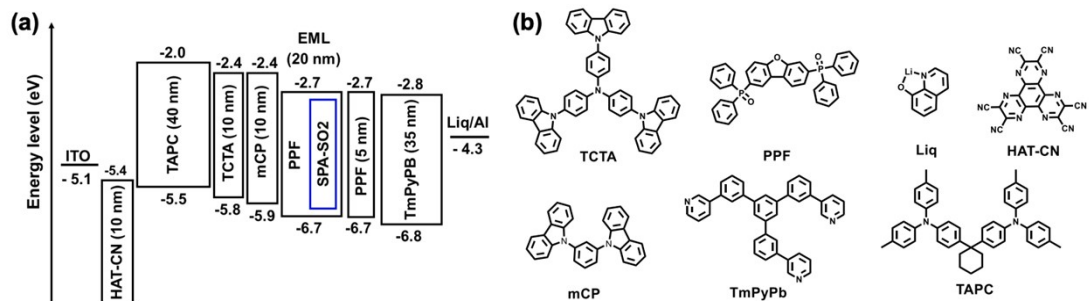


**Fig. S18.** (a) Energy level alignment of the device and (b) the molecular structures of materials in different layers.

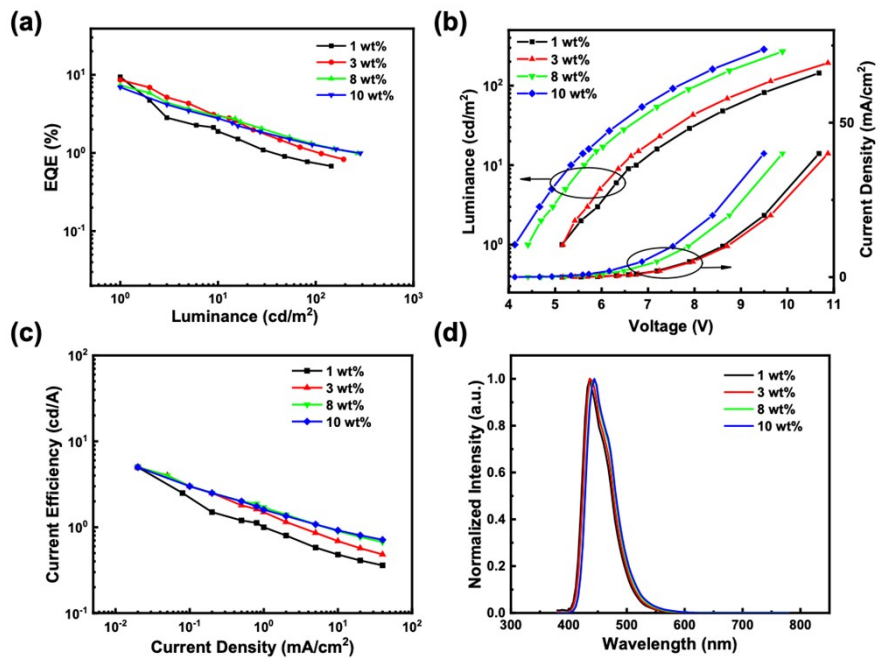


**Fig. S19.** (a) EQE-Luminance curves, (b) Luminance - Voltage-Current density curves, (c) Current efficiency-Current density curves, and (d) Electroluminescence spectra at different doping ratios.

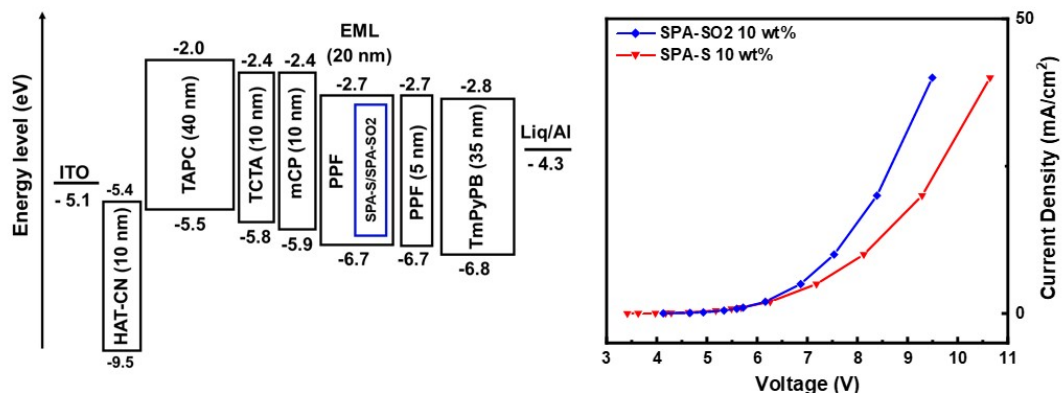


**Fig. S20.** Under the same device structure, the Voltage-Current density curves of SPA-S and SPA-SO2 were tested to compare the charge transport capability.

## 9. Reference

- 1 G. M. Sheldrick, Crystal Structure Refinement with SHELXL, *Acta Crystallogr., Sect. C*, 2015, **71**, 3–8.
- 2 O. Dolomanov, L. Bourhis, R. Gildea, J. Howard and H. Puschmann, OLEX2: A Complete Structure Solution, Refinement and Analysis Program, *J. Appl. Cryst.*, 2009, **42**, 339–341.
- 3 M. J. Frisch, G. W. Trucks, H. B. Schlegel, G. E. Scuseria, M. A. Robb, J. R. Cheeseman, G. Scalmani, V. Barone, G. A. Petersson, H. Nakatsuji, X. Li, M. Caricato, A. V. Marenich, J. Bloino, B. G. Janesko, R. Gomperts, B. Mennucci, H. P. Hratchian, J. V. Ortiz, A. F. Izmaylov, J. L. Sonnenberg, D. Williams-Young, F. Ding, F. Lipparini, F. Egidi, J. Goings, B. Peng, A. Petrone, T. Henderson, D. Ranasinghe, V. G. Zakrzewski, J. Gao, N. Rega, G. Zheng, W. Liang, M. Hada, M. Ehara, K. Toyota, R. Fukuda, J. Hasegawa, M. Ishida, T. Nakajima, Y. Honda, O. Kitao, H. Nakai, T. Vreven, K. Throssell, J. A. Montgomery Jr., J. E. Peralta, F. Ogliaro, M. J. Bearpark, J. J. Heyd, E. N. Brothers, K. N. Kudin, V. N. Staroverov, T. A. Keith, R. Kobayashi, J. Normand, K. Raghavachari, A. P. Rendell, J. C. Burant, S. S. Iyengar, J. Tomasi, M. Cossi, J. M. Millam, M. Klene, C. Adamo, R. Cammi, J. W. Ochterski, R. L. Martin, K. Morokuma, O. Farkas, J. B. Foresman and D. J. Fox, Wallingford, CT, **2016**.
- 4 W. Humphrey, A. Dalke and K. Schulten, VMD: Visual Molecular Dynamics, *J. Mol. Graphics*, 1996, **14**, 33–38.
- 5 T. Lu and F. Chen, Multiwfn: A Multifunctional Wavefunction Analyzer, *J. Comput. Chem.*, 2012, **33**, 580–592.
- 6 X. Gao, S. Bai, D. Fazzi, T. Niehaus, M. Barbatti and W. Thiel, Evaluation of Spin-Orbit Couplings with Linear-Response Time-Dependent Density Functional Methods, *J. Chem. Theory Comput.*, 2017, **13**, 515–524.
- 7 G. Sych, R. Pashazadeh, Y. Danyliv, O. Bezzikonyi, D. Volyniuk, A. Lazauskas and J. V. Grazulevicius, Reversibly Switchable Phase-Dependent Emission of Quinoline and Phenothiazine Derivatives towards Applications in Optical Sensing and Information Multicoding, *Chem. Eur. J.*, 2021, **27**, 2826–2836.